ISSN: 0067-2904

Feature Extraction and Statistical Analysis of EP/TiO_2 & EP/Al_2O_3 Nano-Composite Materials in Acidic Solution

Abdul Adheem Zaily Hameed [1]*, Muzhir Shaban Al-Ani[2], Haval Muhammed Sidqi[3]

[1]*Computer Science Department, College of Computer Science & Information Technology, University of Anbar, Anbar, Ramadi, Iraq*

[2]*Department of Information Technology, College of Science and Technology, University of Human Development, Sulaymaniyah, KRG, Iraq*

[3]*Department of Database, Institute of Computer, University of Sulaimani Polytechnic, KRG Iraq*

Received: 24/4/2024 Accepted: 23/3/2025 Published: 30/3/2026

Abstract

This paper focuses on the study of extracting features from Nano-composites for Alumina (EP/Al_2O_3) and Nano-composites for Titanium (EP/TiO_2) samples before and after immersion in the chemical solution (HNO3) using image processing tools and statistical measures. It is obvious that it is difficult to distinguish the change in the physical properties of the samples before and after immersion in the chemical solution, and it is also difficult even to the naked eyes. Therefore, in this research improvements were made to the image parameters using various techniques to reach the best quality in the image features. Statistical analysis (entropy, standard deviation, mean value, and correlation measures) was applied to obtain the best results in terms of comparing samples before and after immersion in acidic solution. The results obtained indicate that acid immersion affects alumina and titanium samples at different rates, and the effect of acid immersion effect on the case of alumina and the results show that samples of titania nano-composites are more resistant to acid immersion.

Keywords: Surface Structures, Surface Characteristics, Nano-Al_2O_3, Nano-TiO_2, The chemical solution (HNO_3)).

استخلاص الميزات والتحليل الإحصائي للمواد النانوية المركبة EP/TiO_2 و EP/Al_2O_3 في المحلول الحامضي

عبدالعظيم زعيلي المرسومي[1]*، مزهر شعبان العاني [2]،هافال محمد صديق[3]

[1] قسم غلوم الحاسبات، كلية علوم الحاسوب وتكنولوجيا المعلومات، جامعة الانبار، الانبار، العراق

[2]قسم تكنولوجيا المعلومات، كلية العلوم والتكنولوجيا، جامعة التنمية البشرية، السليمانية، العراق

[3]قسم قواعد البيانات، معهد الحاسوب، جامعة السليمانية التقنية، حكومة إقليم كردستان، العراق

* Email: ab72d74@uoanbar.edu.iq

الخلاصة

يركز هذا البحث على دراسة استخلاص الخصائص من المركبات النانوية لعينات الألومينا (EP/Al_2O_3) والمركبات النانوية لعينات التيتانيوم (EP/TiO_2) قبل وبعد الغمر في المحلول الكيميائي (HNO3) باستخدام أدوات معالجة الصور والمقاييس الإحصائية . ومن الواضح أنه من الصعب تمييز التغير في الخواص الفيزيائية للعينات قبل وبعد غمرها في المحلول الكيميائي، كما أنه من الصعب حتى بالعين المجردة. ولذلك، تم في هذا البحث إجراء تحسينات على معالم الصورة باستخدام تقنيات مختلفة للوصول إلى أفضل جودة في ميزات الصورة. تم تطبيق التحليلات الإحصائية (الإنتروبيا، الانحراف المعياري، القيمة المتوسطة ومقاييس الارتباط) للحصول على أفضل النتائج من حيث مقارنة العينات قبل وبعد الغمر في المحلول الحمضي. تشير النتائج المتحصل عليها إلى أن الغمر بالحمض يؤثر على عينات الألومينا والتيتانيوم بنسب مختلفة، وتأثير تأثير الغمر بالحامض على حالة الألومينا وأظهرت النتائج أن عينات مركبات التيتانيوم النانوية أكثر مقاومة للغمر بالحامض.

1. Introduction

Nanotechnology and nanoscience are polymers that have been made by chemists, which are large molecules made up of nanoscale subunits. Nanotechnology has been used to create the tiny features of computer chips for years [1]. Technology of nanoparticles (nanotechnology) related to the science that is concerned with the study of processing on the atomic and molecular scale, leading to a technical revolution in many fields and wide applications [2]. A nanoparticle is generally denoted as a particle of diameter between 1 and 100 nanometres [3]. It is difficult to predict which size of a certain material, their characteristics will change; this threshold also depends on the type of material and characteristic [4].

Image processing is one of the specializations of computer science and informatics, and it has wide applications. In addition, it enters into all other disciplines [5]. The first step in image processing is to capture the image using a digital camera, which in turn converts the image into digital values [6]. After that, the required processing is carried out on the image using complex algorithms to obtain the required features [7]. Digital image processing is the process of transforming an image into a digital form and performing certain operations to obtain useful information from it [8]. The image processing system generally treats all images as 2D signals when it applies certain processing methods [9]. The most important part of digital image processing is how to adapt different methods in the procedure to generate significant features [10].

2. Nano-Al_2O_3 and Nano-TiO_3

Nano alumina (Nano-Al_2O_3) is used as a support material, and it is one of the important ceramic oxides because of its high mechanical and thermal properties such as thermal resistance, high thermal stability and high mechanical resistance. An American laboratory powder type (Gamma) was used, and Table 1 shows the most important properties of alumina used.

Table 1: The specification of alumina dioxide nanoparticles

Product name	Color	PH Value	Particle size	Al_2O_3Content	Density
Alumina powder Nano Grade	White	6.6	20nm(Gamma)	99.99%	3.89gm/cm^3

Titanium Oxide (TiO_2) is available in the form of Nano or Nano-crystals with a large surface area. They have magnetic properties. Titanium belongs to block D, period 4, while oxygen belongs to block P, period 2 of the periodic table. Titanium dioxide is also known as flamingo, rutile, titanium dioxide, and titanium dioxide. Titanium oxide nanoparticles are

known for their ability to inhibit bacterial growth and prevent the formation of cell structures. Table 2 shows the most important properties of titanium used.

Table 2 Specification of titanium dioxide nanoparticles

Product name	Color	Particle size	TiO_2 content
TiO_2 powder Nano grade	White	45 nm	≥99.8%

This research focuses on hybridizing image processing and statistical analysis in order to obtain efficient results in comparing samples before and after acid immersion.

3. Related Works

This section is divided into two subsections: nanoparticle materials and image surface features extraction.

4. Nanoparticle Materials

Below are ten papers related to nanoparticle materials.

Shuai Wang et al. [11] described an efficient method of the addition of 0.1% nanoparticles of iron oxide to a carbon-negative enzymatic construction material (ECM) then under ambient conditions applied rapid curing. This method indicated that an optimal strength in 12 hours was obtained via low-power laser.

Amru Daulay et al. [12] added KBr during the reduction of the magnesiothermic method in the Si nanoparticles, which was an effective method. Diffraction of X-ray confirmed the Si nanoparticles crystalline nature with a cubic structure of silicon lattice, and analysis of scanning electron microscopy indicated the spherical morphology of nanoparticles.

Thanida Chuacharoen et al. [13] synthesized the loaded curcumin with zein nanoparticles using a dispersion of liquid-liquid method and incorporated into zein coating material. The obtained result indicated that curcumin was entrapped in zein nanoparticles at 100 μg/ml was more effective than the solution of free curcumin at the same amount.

Philip Adebayo et al. [14] investigated the effect of adding high-conductivity nanoparticles with the uniform magnetic field on the rate of melting of Octadecane PCM. The obtained result indicated that the liquid fraction decreased by 43%, and also the melting rate.

Ji Zhang et al. [15] proposed an integration of Al_2O_3 nanoparticles and a novel fin structure to improve the performance of melting of phase change materials for thermal energy storage systems. The percentages 3%, 6%, and 9% of Al_2O_3 nanoparticles were integrated into the phase change materials, then the obtained results indicated that the melting time is decreased by 13.1%, 15.6%, and 18.8%, respectively.

Luying Liu et al. [16] showed that releasing NO signaling molecules and scavenging harmful ROS affected the dual-catalyzed CuTPP/TiO_2 film and regulated the microenvironment surrounding the implanted device. This dual-catalyzed endothelial bionic method provided a promising solution to clinical problems affecting blood-contact devices and provided a new basis for further development of catalytic surface biomaterials.

Xiaoguang San et al. [17] demonstrated that WO_3 nanoparticles have been successfully bonded on SiO_2/Si equipped with interdigitated Pt electrodes by heating tungsten filaments using a vacuum chamber. The structure of the WO_3 nanoparticles obtained was distinguished using field emission scanning electron microscopy and X-ray diffractometer. The results show that these nanoparticles have a spherical structure and that their size depends on the deposition pressure.

Bingxue Sun et al. [18] tried to damp the size variation of the phosphor-based anode in order to improve its electrical conductivity. Nickel phosphide (NiP) nanoparticles were

encapsulated in the lamellar carbon layer by solvothermal combined thermal decomposition reaction. In which the size expansion of NiP anode can be reduced during the cycling process.

Ahmad M. Al-Thobity et al. [19] evaluated the effect of silicon dioxide nanoparticles on the flexural toughness of heat-polymerized denture. Among 167 studied papers, five were satisfied with the inclusion standard and were added for meta-analysis and data analysis.
S.S. Tuly et al. [20] studied the effect of modifications of the hollow circular fin (HCF), inner sidewall reflector (ISR), mixed nanoparticle PCM (nano-PCM) and phase change material (PCM) on the thermodynamic performance of solar stills. The obtained result indicated that the cumulative action of ISR, HCF and PCM leading to an increase in productivity of 51.8% compared to the conventional method.

5 . Image Surface Features

Below are ten published papers related to the image surface features subject.
Przemysław Podulka [21] proposed an analysis to improve the use of image evaluation in the description of material properties. The results were analyzed with the characterization of the surface topographic image. He found that wavelet filtering approaches could be useful in evaluations of selected texture features of the surface, such as size or texture distributions or processing trace distances.
Kirandeep Kaur et al. [22] implemented data simulation for carbon steel infrared thermography. Principle Component Analysis (PCA) is used for data processing in order to reach significant results. The second component PCA led to small defects in the characteristic and improved the value of signal to noise ratio compared to other PCA components.
Nathan D. et al. [23] obtained feature extraction of texture image via grey level co-occurrence matrix. Different features of texture image such as contrast, correlation, homogeneity, and energy, are obtained via different sampling. In addition, the relationship between image texture features and surface roughness was measured.
Camila Cesar et al. [24] described and identified many structures: bright-haloed spot, dark spot, ringed spot, dark-haloed spot, inverted spot, and bright spot and banded spot. They applied an approach to verify the multifiltering process with high resolution to obtain color contrast high sensitivity. They obtained an efficient evaluation of features using spectral analyses.
Bishal Roy et al. [25] applied cloud computing on Google Earth Engine using filtering and analyzing with statistical measures. surface vegetation coverage and land surface temperature were two main factors affecting each other during the implementation. The obtained results indicated that the northeastern region had the greatest variations in surface temperature because of higher vegetation coverage area.
Mona Alghamdi et al. [26] demonstrated different deep learning neural networks methods, which are vital for the extraction of high-level discriminatory abstract features. In addition, several similarity measures were used for the matching process. The obtained results indicated that joint patterns and nails play an important role in the person identification framework.
Dimas Firmanda Al Riza et al. [27] Evaluated both color and texture characteristics of the images in order to develop a maturity prediction model. The results obtained showed that the combination of texture features and color features of reflectance image will increase the R_2 of the partial least squares regression up to 0.97 and 0.99 for the Brix prediction and PH prediction, respectively with a root mean square error of 0.5 for both.
Chen Zhao et al. [28] developed an automated approach for lung parenchyma segmentation in CT chest images, then analyzed the texture characteristics of segmented regions to help

radiologists in the diagnosis of COVID-19. The obtained results denoted that the proposed segmentation method achieved sensitivity, Dice similarity, specificity, and average distance error of 0.9840, 0.9796, 0.9954, and 0.0318 mm, respectively.
Tiril Aurora Lintvedt et al. [29] studied three manual scanning methods: line scan of the belly line scan of loin, and sinusoidal scan of the belly at exposure times of 2 seconds and 4 seconds. High performance was obtained for the test set, but while Raman had stable biases and low value for the test set, the biases were high and varied for the near infrared measures.
Elham Avard et al. [30] studied the radiomic characteristics and developed a machine learning algorithm for the separation of myocardial infarction. All images were segmented and verified simultaneously by two cardiac imaging experts. Then, feature extraction was performed on the entire left ventricular myocardium in the end-diastolic volume phase. The radiological analysis indicated an optimal performance obtained using machine learning approach.

6. Methodology

This research methodology is divided into two parts: the sample casting process and the image processing section.

6.1 Sample Casting Process

The main method of sample preparation and casting consists of the following (Fig.1):
Prepare the weighted quantity for the required ratio of epoxy and hardener added in a ratio of (3:1).

- Preparing the weighted amount of the material (aluminum oxide and titanium dioxide particles) nanoparticles and natural hybrids, with a weight fraction of 4%. The reinforcing materials and matrix were mixed at room temperature. The weighted proportions of the reinforcement and the matrix were mixed together in a special bowl using an electric mixer until homogeneity was achieved, then the hardener was added to the mixture and the mixing process took place for 3 minutes.
- The liquid mixture has been poured in the middle of the mold so that it is distributed to all areas of the mold continuously so the mold is filled to the required level.
- The mold is left for (48) hours until it hardens completely, then leave the mold in the oven at a temperature of (50 °C) for (5) hours to complete its ability to form, then the sample is cut from one of them. Diagonally at an angle of 45 degrees.
- Three digital images of the sample surface, sample base, and sample tilt are taken with a Nokia camera.
- The chemical solution (HNO_3) is normalized to (N) of degree 1 (N = 1). The normality of the solution combines evenly to understand the effect of these solutions on the samples.
- The samples are immersed in the acidic solution (HNO_3) for a period of 15 days, then photographs are retaken in the same way as before.

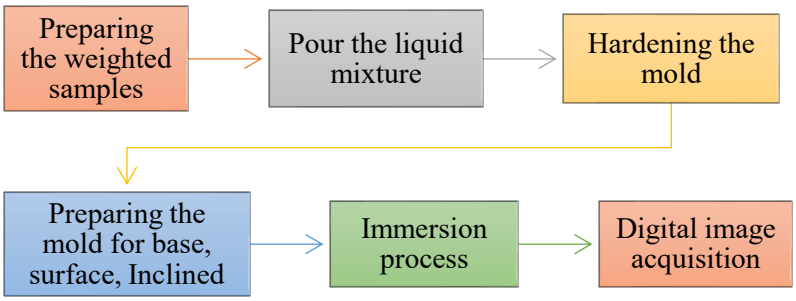

Figure 1: Sample Casting Process

6.2 Image Processing Procedure

After the sample casting process is performed, the image processing procedure will be started. This procedure contains six steps (Fig.2):

- Image Acquisition: after preparing the molding samples, a high resolution camera is used to take photos of the casting samples, then these images are received by the computer to be processed.
- Image Preprocessing: preparing and organizing the images, then converting these images into a standard size 100*100 pixels.
- RGB to Gray Scale: as this work focuses on surface structure, it is necessary to convert color images into gray scale images of 256 levels.
- Adjust Image Intensity: to adjust it is important to increase the low-contrast grayscale of the image by generating a new mapping of pixel values to fit the overall intensity range from 0 to 255.
- Contrast Enhancement: this process aims to increase the ability of the approach to distinguish between the gray levels or objects, and it is implemented via adjacent structures.
- Contrast Highlighting: this process aims to differentiate between low contrast and high contrast.
- Contour Measures: when the low contrast pixels are separated from high contrast pixels, it is easy to contour the objects in this process.
- Statistical Measures: many statistical measures are implemented for surface structure analysis. These functions are Entropy, correlation, standard deviation, and mean values.

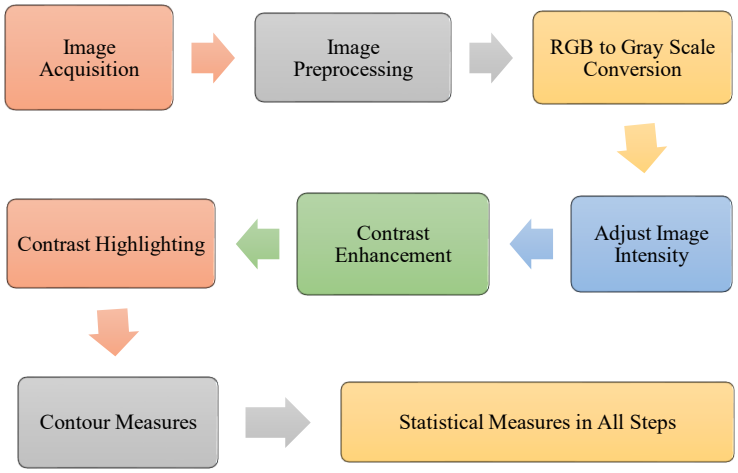

Figure 2: image processing procedure

7. Results and Discussion

In order to explain the obtained results in this work, it is important to guide the implemented procedure step by step. Two types of molding were used: nano-alumina and nano-titanium dioxide. Three types of images were used, lower surface or base images (two images), upper surface images (two images), and inclined images (two images). After converting color images into grayscale, some types of processing were applied to enhance images; adjust image intensity, contrast enhancement, and contrast highlighting. Finally, statistical measures were applied to extract the features and distinguish the effect of acid immersion of the sample.

7.1 Image Processing

Fig.3 shows the gray scale of nano-alumina image before and after immersion and their histogram. In this figure, you cannot distinguish between these two images in the normal eyes, so a number of operations were applied to improve the image enhancement. In addition, looking at the histogram, you can see that there is a displacement in the histogram to the right after the immersion process, which means there are more pixels corresponding to the low values, and this indicates the effect of acid immersion on the sample.

a) gray scale image before immersion **b)** gray scale image after immersion

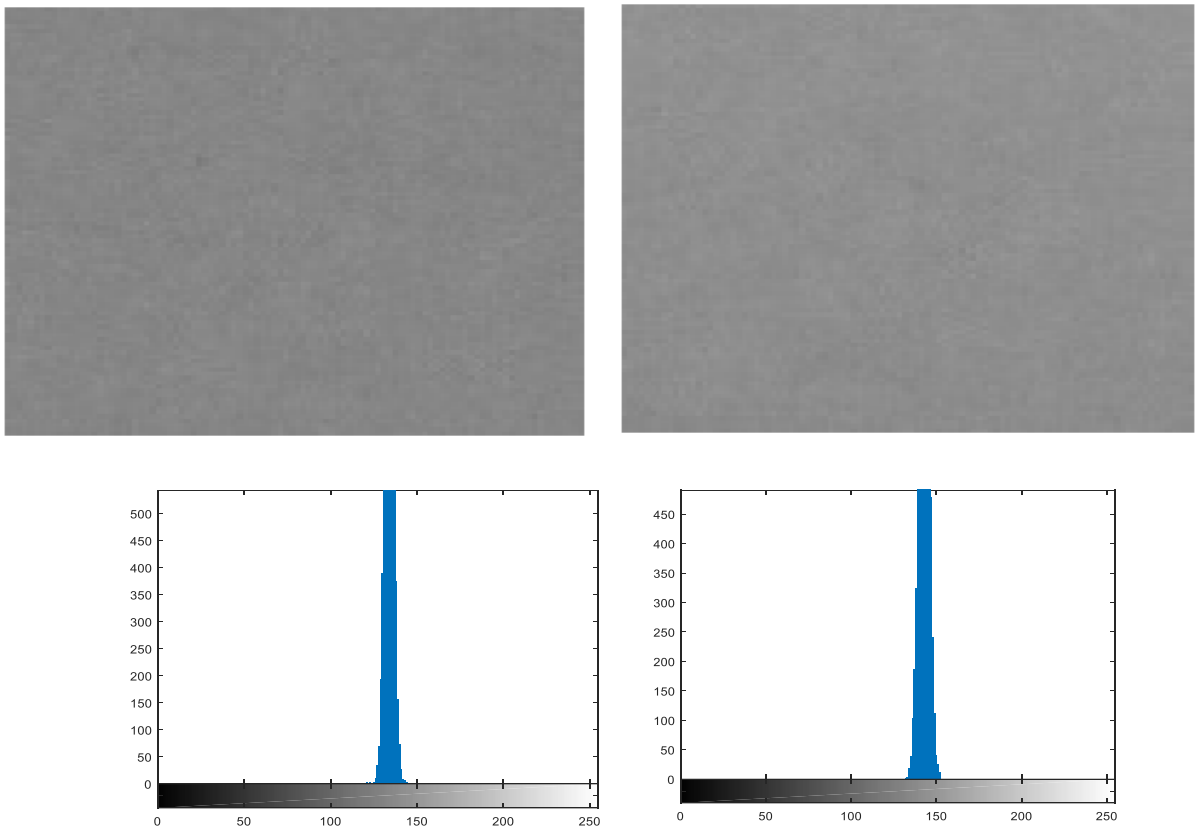

c) histogram of image a **d)** histogram of image b

Figure 3: gray scale image before and after immersion and their histogram

Figure 4 demonstrates the first enhancement process applied, adjusting the image intensity before and after immersion and their histogram. This process is used to enhance the quality intensity of the image. Comparing the two images in this figure, it is possible to notice the acid effect clearly in the upper right corner, and this is confirmed by the histogram before and after the acid immersion, there is a clear difference in the distribution after the acid immersion.

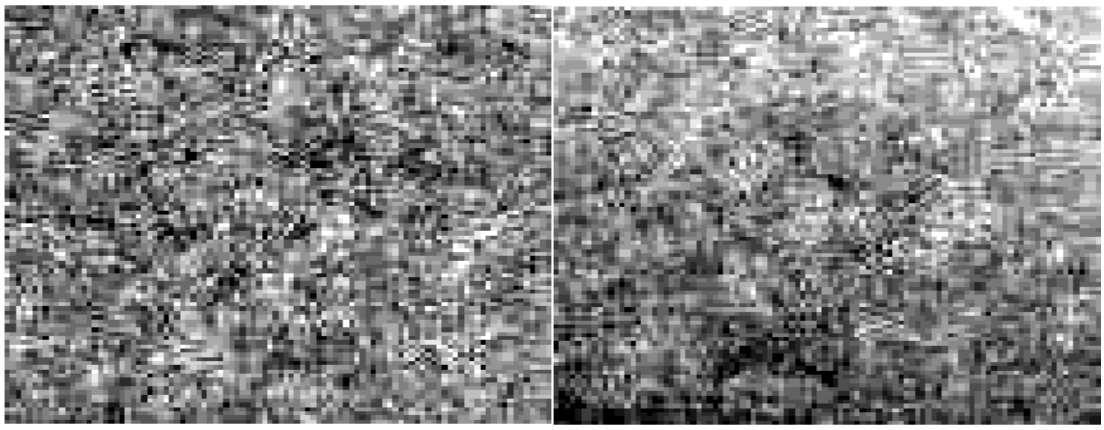

a) adjusted image before immersion **b)** adjusted image after immersion

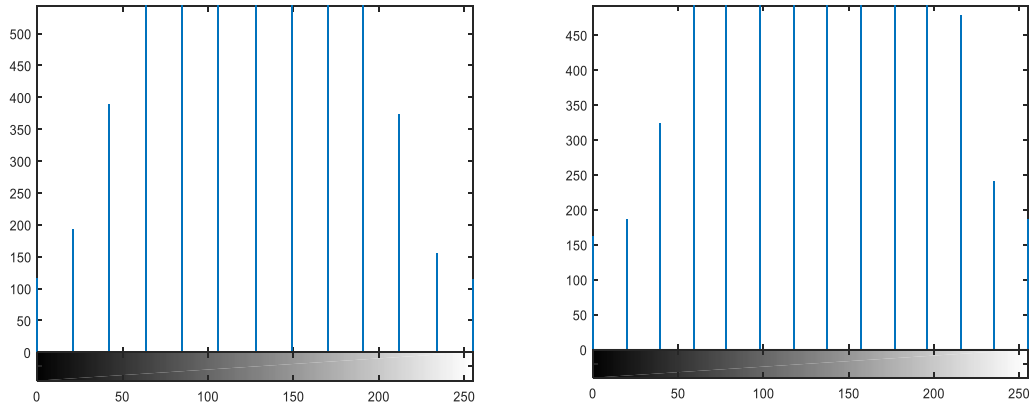

c) histogram of image a **d)** histogram of image b

Figure 4: adjust image intensity before and after immersion and their histogram

Figure 5 clarifies that there is a contrast image enhancement before and after immersion and their histogram. This process is achieved via applying the histogram equalization function, which adjusts and enhances the image contrast. Then the image can be represented by a narrow range of intensity values. It is clear from the histogram that this process has more effect than the previous one, in addition, there is a slight difference between before immersion and after immersion.

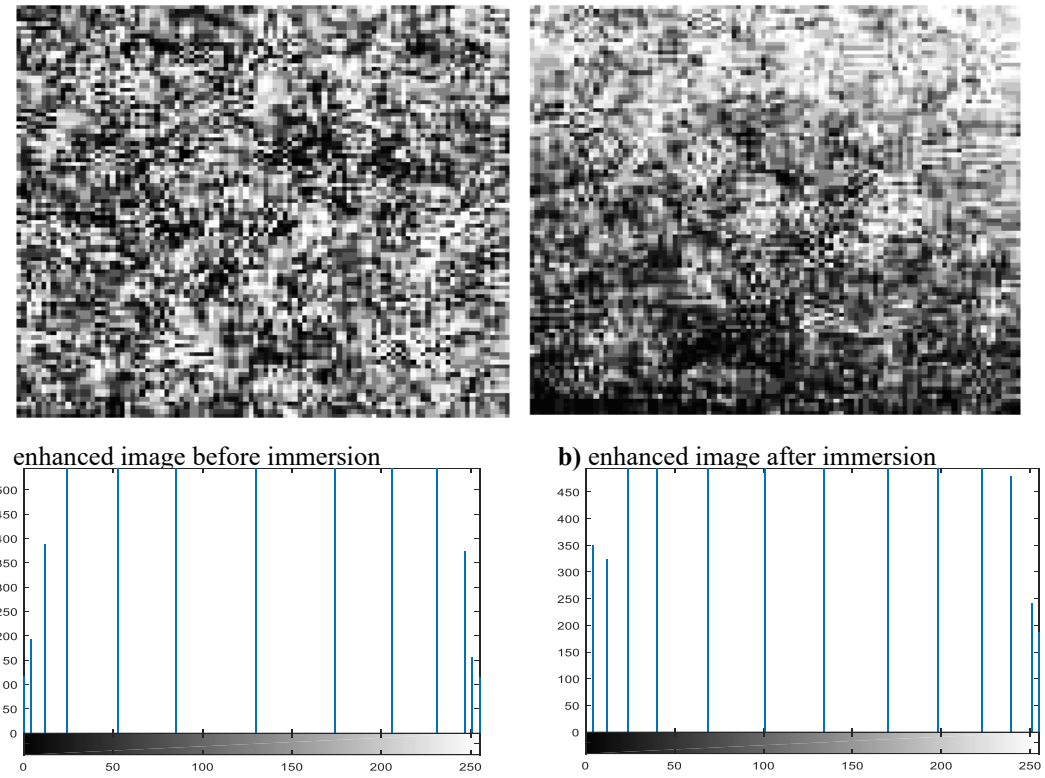

a) enhanced image before immersion **b)** enhanced image after immersion

c) histogram of image a **d)** histogram of image b

Figure 5: contrast enhancement image before and after immersion and their histogram

Figure 6 presents the area of contrast image highlights before and after immersion. Contour and full contour functions are used to reproduce contrast highlighting of images to extract the effect of acid immersion on the sample. It is clear that there is a significant effect on the immersed sample compared with the original sample.

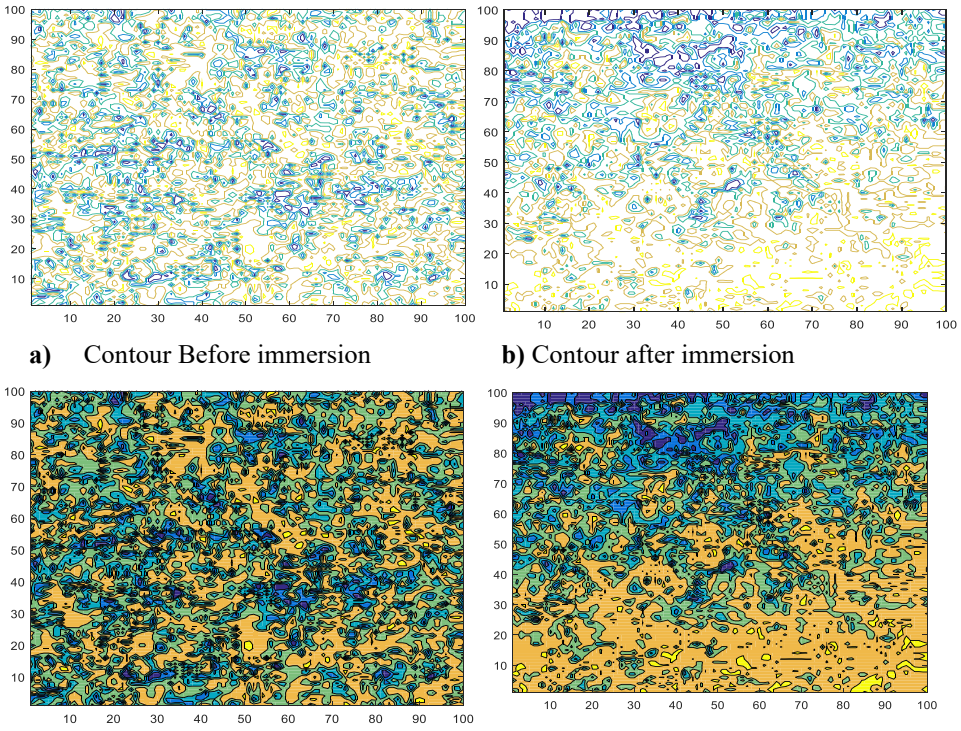

a) Contour Before immersion **b)** Contour after immersion

c) full contour Before immersion **d)** full contour after immersion

Figure 6 contrast highlighting image before and after immersion

7.2 Statistical Measures

After finalizing the image processing task, and to facilitate comparison using statistical measures, some definitions of the functions used are summarized. EntropyB1 and EntropyA1 are the entropy measures of the image before immersion and after immersion respectively. Standard DeviationB1 and Standard DeviationA1 are the Standard Deviation measures of the image before and after immersion respectively. Mean ValueB1 and Mean ValueA2 are the mean value measures of the image before and after immersion respectively. In addition, the correlation process is applied to measure the effect of the immersion process.

Figures 7-10 show statistical measures of nano-alumina (alumina) and nano-titanium (Ttitania) of images before and after immersion. Statistical measures are applied on the two sample images (image1 and image2) of each type.

Any change that occurs automatically in a physical system must be accompanied by an increase in entropy, which is used for measuring the amount of information within an image. The difference between the entropy values before and after immersion for alumina and titania is clear, as shown in Fig. 7.

The mean value of the entropy of the alumina before and after the immersion is 3.720395833 and 4.659725, respectively, indicating a significant difference between the two samples. Furthermore, the average value of titania entropy before and after immersion is 3.326470833 and 3.524520833 respectively, indicating a significant difference between the two samples. On the other hand, the variation of the alumina percentage of the entropy is 25.2481 % while the average variation of the titanium percentage of the entropy is 5.9538 %.

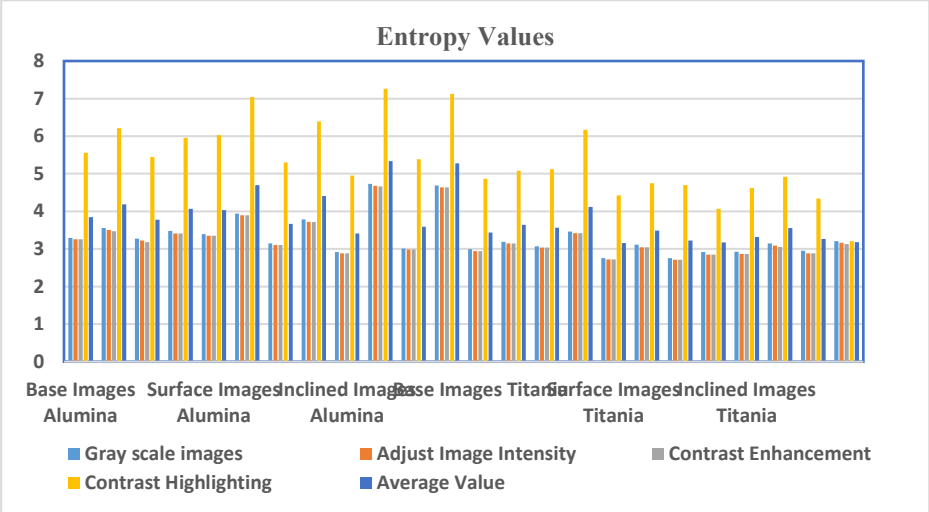

Figure7: Entropy measures of images before and after immersion

Standard deviation measures the deviation of the measured values from their mean. When standard deviation is high, the values are scattered and at the same time far from the mean. Low variance or standard deviation means the pixel intensities are closer to the mean, and high variance means the pixel intensities are far from the mean. In addition, contrast is high for images with high standard deviation values.

Fig.8 demonstrates the standard deviation measures of images before and after immersion for alumina and titania. The average standard deviation values of alumina before and after immersion are 47.48563333 and 51.27899167 respectively, this indicates that there is a significant difference between the two samples. In addition, the average standard deviation value of titania before and after immersion are 47.88860417 and 47.96329583 respectively, this indicates that there is a significant difference between the two samples. On the other

hand, the standard deviation of alumina percentage change is 7.9884 %. In comparison, the mean titania percentage change is 0.1557 %, so, this indicates that titania samples lead to very small effects via acid immersion.

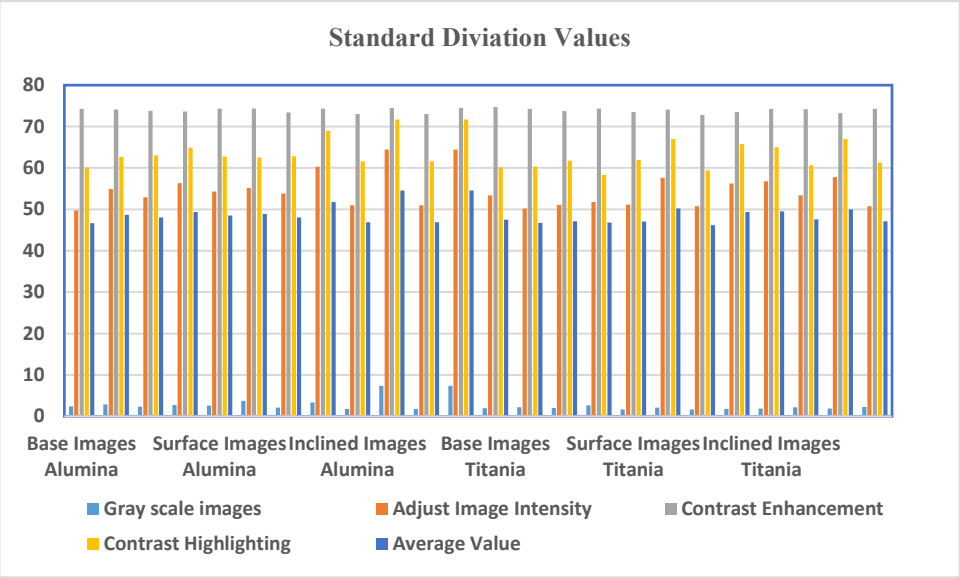

Figure 8: Standard Deviation measures of images before and after immersion

Mean value is represented by the sum of pixel values divided by the total number of pixel values. Mean value gives the contribution of individual pixel intensity for the entire image. Fig.9 illustrates the mean value measures of images before and after immersion for alumina and titania. The average mean value of alumina before and after immersion are 134.3459333 and 140.2490333, respectively, indicating a significant difference between the two samples. In addition, the average mean value of titania before and after immersion are 141.7929667 and 143.5906, respectively, this indicates that there is a significant difference between the two samples. On the other hand, the mean alumina percentage change is 4.2090 % while the mean titania percentage change is 1.2678 %, so, this indicated the titania samples are less affected by acid immersion.

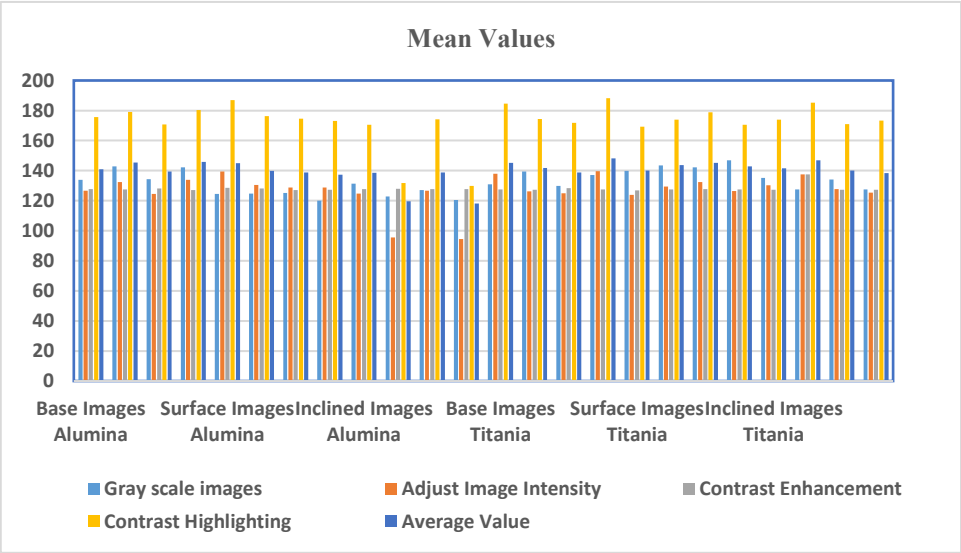

Figure 9: Mean value measures of images before and after immersion

The correlation was measured between images before and after immersion for both alumina and titania as shown in Fig. 10. Then the average correlation values are calculated

for Alumina before and after immersion is 0.1851125, and for titania before and after immersion is 0.063075. In order to demonstrate the final comparison, the average value was calculated to compare both Alumina and Titania. It is clear from the figure that the average correlation value of alumina is significantly greater than that of the average correlation value of titania. So, it is clear that the acid immersion has more effect on alumina compared to titania. In addition, there is a big effect of the inclined section image after immersion for both Alumina and Titania.

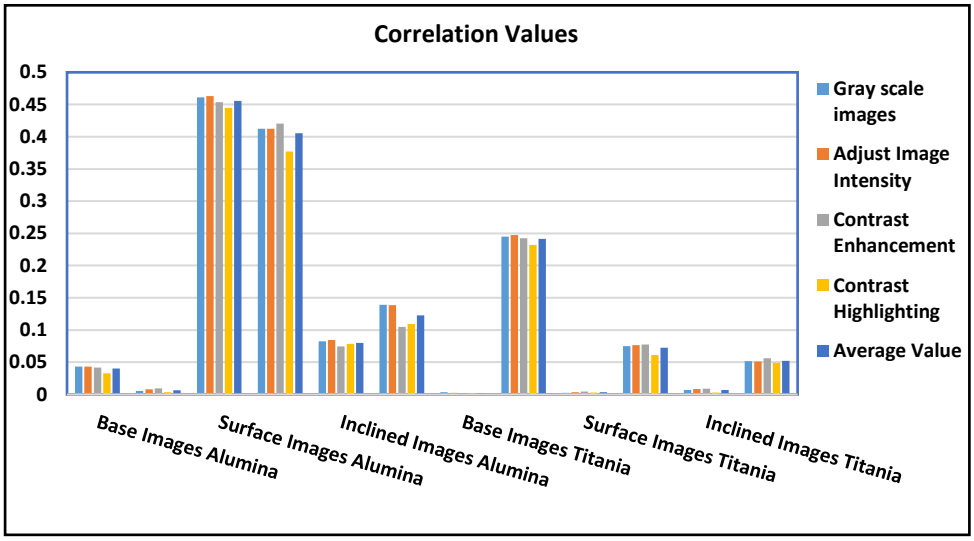

Figure10: Correlation measures of images before and after immersion

8. Conclusions

In this research, the improvement in image processing was combined with statistical analyses to reach an efficient way to demonstrate the effect caused by acid immersion on both Alumina and titania samples. This integration of these technologies leads to obtaining effective surface features to reach an efficient comparison between samples.

Entropy and standard deviation both values are slightly increased in the immersed sample image. Still, the mean value in the immersed sample image is significantly different from the original sample image. This is true for both image1 and image2 with slight difference.

Based on the results obtained through statistical analyses and calculations, it was found that both alumina and titanium are affected by acid immersion in different proportions, and that alumina is affected more in acid immersion compared to Titania. So, this indicates that the resistance of titanium to acid immersion is stronger than the resistance of alumina to acid immersion.

References

[1] A. A. Z. Hameed, M. A. Shahood, and M. Khalaf, "Study of the effect of heat curing on the surface texture of (UP / Micro-MgO) and (UP / Nano-MgO) composites: Image analysis," in *AIP Conference Proceedings*, vol. 2400, p. 030021, 2022.

[2] A.-A. Z. Hameed, M. S. Al-Ani, and F. H. Anter, "Applying image processing tools to analyze the surface characteristics of nano alumina (NANO AL2O3) and nano titanium (NANO TIO2)," *J. Teknologi (Sci. & Eng.)*, vol. 80, no. 4, pp. 55–65, Jul. 2018.

[3] A.-A. Z. Hameed and M. S. Al-Ani, "The effect of acidic solution (H2SO4) on the nano composites materials (EP/ Nano-SiO2): Image analysis study," *Rev. aus.*, no. 26.2, pp. 501–510, 2019.

[4] A. A. Z. Hameed, M. S. Al-Ani, and R. H. Khalaf, "Study the effects of gamma radiation on nano composite material (Nano MgO): Image analysis," *NeuroQuantology*, vol. 20, no. 4, pp. 578–587, 2022.

[5] M. S. Al-Ani and S. M. H. "3D visualization based on surface estimation techniques," *Int. J. Adv. Eng. Technol.*, vol. 6, no. 2, pp. 606–612, May 2013.
[6] M. S. Al-Ani and S. M. H., "Medical image enhancement based on an efficient approach for adaptive anisotropic diffusion," *Int. J. Adv. Eng. Technol.*, vol. 6, no. 3, pp. 1424–1430, May 2013.
[7] M. S. Al-Ani and Q. Al-Shayea, "An efficient approach to 3D image reconstruction," *Int. J. Comput. Sci. Netw. Secur. (IJCSNS)*, vol. 16, no. 8, pp. 35–41, 2016.
[8] M. S. Al-Ani and K. M. A. Alheeti, "Precision statistical analysis of images based on brightness distribution," *Adv. Sci. Technol. Eng. Syst. J.*, vol. 2, no. 4, pp. 99–104, 2017.
[9] B. A. Mohammed and M. S. Al-Ani, "Digital medical image segmentation using fuzzy C-means clustering," *UHD J. Sci. Technol. (UHDJST)*, vol. 4, no. 1, pp. 51–58, 2020.
[10] S. M. Nejrs and M. S. Al-Ani, "Face image classification based on feature extraction," *Solid State Technol.*, vol. 63, no. 6, Dec. 2020.
[11] S. Wang, S. Scarlata, and N. Rahbar, "Curing and self-healing of enzymatic construction materials using nanoparticles," *Cell Rep. Phys. Sci.*, vol. 3, no. 9, Art. no. 101039, Sep. 2022.
[12] A. Daulay, Andriayani, Marpongahtun, and S. Gea, "Synthesis Si nanoparticles from rice husk as material active electrode on secondary cell battery with X-ray diffraction analysis," *S. Afr. J. Chem. Eng.*, vol. 42, pp. 32–41, Oct. 2022.
[13] T. Chuacharoen and C. M. Sabliov, "Development of coating material by incorporating curcumin-loaded zein nanoparticles to maintain the quality of mango (Mangifera indica L. cv. Nam Dokmai)," *J. Agric. Food Res.*, vol. 10, Art. no. 100444, Dec. 2022.
[14] P. Adebayo and A. Yehya, "The effect of combining magnetic field and high-conductivity nanoparticles on the fusion rate of a phase change material," *Energy Convers. Manage.: X*, vol. 16, Art. no. 100314, Dec. 2022.
[15] J. Zhang, Z. Cao, and C. Wen, "Improving the melting performance of phase change materials using novel fins and nanoparticles in tubular energy storage systems," *Appl. Energy*, vol. 322, Art. no. 119416, Sep. 2022.
[16] L. Liu et al., "Dual-catalytic CuTPP/TiO2 nanoparticles for surface catalysis engineering of cardiovascular material," *Mater. Today Bio*, vol. 17, Art. no. 100494, Dec. 2022.
[17] X. San et al., "Ultrasensitive and selective sensing material of ultrafine WO3 nanoparticles for the detection of ppb-level NO2," *Resour. Chem. Mater.*, vol. 1, no. 3–4, pp. 261–267, Sep.–Dec. 2022.
[18] B. Sun and J. Ni, "NiP nanoparticles encapsulated in lamellar carbon as high-performance anode materials for sodium-ion batteries," *Electrochem. Commun.*, vol. 141, Art. no. 107344, Aug. 2022.
[19] A. M. Al-Thobity and M. M. Gad, "Effect of silicon dioxide nanoparticles on the flexural strength of heat-polymerized acrylic denture base material: A systematic review and meta-analysis," *Saudi Dent. J.*, vol. 33, no. 8, pp. 775–783, Dec. 2021.
[20] S. S. Tuly et al., "Investigation of a modified double slope solar still integrated with nanoparticle-mixed phase change materials: Energy, exergy, exergo-economic, environmental, and sustainability analyses," *Case Stud. Therm. Eng.*, vol. 37, Art. no. 102256, Sep. 2022.
[21] P. Podulka, "Application of image processing methods for the characterization of selected features and wear analysis in surface topography measurements," *Procedia Manuf.*, vol. 53, pp. 136–147, 2021.
[22] K. Kaur and R. Mulaveesala, "Active infrared imaging for estimation of sub-surface features in a steel material," *Procedia Comput. Sci.*, vol. 171, pp. 1204–1211, 2020.
[23] D. Nathan, G. Thanigaiyarasu, and K. Vani, "Study on the relationship between surface roughness of AA6061 alloy end milling and image texture features of milled surface," *Procedia Eng.*, vol. 97, pp. 150–157, 2014.
[24] C. Cesar et al., "Seasonal southern circum-polar spots and araneiforms observed with the colour and stereo surface imaging system (CaSSIS)," *Planet. Space Sci.*, vol. 224, Art. no. 105593, Dec. 2022.
[25] B. Roy and E. Bari, "Examining the relationship between land surface temperature and landscape features using spectral indices with Google Earth Engine," *Heliyon*, vol. 8, no. 9, Art. no. e10668, Sep. 2022.

[26] M. Alghamdi, P. Angelov, and L. P. Alvaro, "Person identification from fingernails and knuckles images using deep learning features and the Bray-Curtis similarity measure," Neurocomputing, vol. 513, pp. 83–93, Nov. 2022.

[27] D. F. A. Riza, C. Rulin, N. T. T. Tun, P. P. L. Yi, A. A. Thwe, K. T. Myint, and N. Kondo, "Mango (Mangifera indica cv. Sein Ta Lone) ripeness level prediction using," J. Agric. Food Res., vol. 11, Article 100477, 2023.

[28] C. Zhao, Y. Xu, Z. He, J. Tang, Y. Zhang, J. Han, Y. Shi, and W. Zhou, "Lung segmentation and automatic detection of COVID-19 using radiomic features from chest CT images," Pattern Recognit., vol. 119, Article 108071, Nov. 2021.

[29] T. A. Lintvedt, P. V. Andersen, N. K. Afseth, K. Heia, S.-K. Lindberg, and J. P. Wold, "Raman spectroscopy and NIR hyperspectral imaging for in-line estimation of fatty acid features in salmon fillets," Talanta, vol. 254, Article 124113, Mar. 2023.

[30] E. Avard, I. Shiri, G. Hajianfar, H. Abdollahi, K. R. Kalantari, G. Houshmand, K. Kasani, A. Bitarafan-rajabi, M. R. Deevband, M. Oveisi, and H. Zaidi, "Non-contrast Cine Cardiac Magnetic Resonance image radiomics features and machine learning algorithms for myocardial infarction detection," Comput. Biol. Med., vol. 141, Article 105145, Feb. 2022.